Star confusion effect on SIM PlanetQuest astrometric performance

C. Zhai, J. Yu, M. Milman, N. Fathpour,
M. Morales, B. Nemati, M. Regehr, M. Heflin, and L. Sievers

ABSTRACT

SIM PlanetQuest will measure star positions to an accuracy of a few microarcseconds using precise white light fringe measurements. One challenge for SIM observation scenario is "star confusion," where multiple stars are present in the instrument field of view. This is especially relevant for observing dim science targets because the density of number of stars increases rapidly with star magnitude. We study the effect of star confusion on the SIM astrometric performance due to systematic fringe errors caused by the extra photons from the confusion star(s). Since star confusion from multiple stars may be analyzed as a linear superposition of the effect from single star confusion, we quantify the astrometric errors due to single star confusion surveying over many spectral types, including A0V, F0V, K5III, and M0V, and for various visual magnitude differences. To the leading order, the star confusion effect is characterized by the magnitude difference, spectral difference, and the angular separation between the target and confusion stars.

Strategies for dealing with star confusion are presented. For example, since the presence of additional sources in the field of view leads to inconsistent delay estimates from different channels, with sufficient signal to noise ratio, the star confusion can be detected using chi-square statistics of fringe measurements from multiple spectral channels. An interesting result is that the star confusion can be detected even though the interferometer cannot resolve the separation between the target and confusion stars when their spectra are sufficiently different. Other strategies for mitigating the star confusion effect are also discussed.

1. INTRODUCTION

SIM PlanetQuest mission, designed to measure star positions to micro arcsecond accuracy, requires very precise fringe measurements.[1,2] One source of systematic error in fringe measurement comes from observing a confusion field, where multiple stars appear in the instrument field of view. The additional stars generate fringes that are incoherently superposed to the nominal fringes from the target star leading to systematic error in the fringe measurement. Even though, the narrow angle science target stars are relatively bright stars, several SIM key projects, such as microlensing, dynamical observations of galaxies and observation of the globular clusters requires observing confusion fields. The situation gets worse for dimmer target stars because the number density of the stars increases rapidly as the visual magnitude.[3] Star confusion can greatly affect the SIM astrometric performance.

In this article, we report the effect of the confusion field on the fringe measurement. In a parallel study,[4] the effect of the confusion field on the angle tracking camera performance has been quantified, where the angle tracking error due to confusion is mostly under 100 mas. Angle tracking error can cause the fringe measurement error by shifting the image on the fringe camera. We found that 100mas angle tracking error leads to only a few picometer astrometric error. Therefore, in our study, we simply assumed zero angle tracking error. In general, the star confusion effect depends on the angular separations, the relative brightness and the spectral difference between the targ~~et and confu~~sion stars. Because the confusion effect due to multiple stars can be analyzed as a superposition of the effect of each individual star confusion. We quantify the impact from a single confusion star at a range of separations with difference spectral types and visual magnitudes.

Strategies for dealing with star confusion are presented. With multiple spectral channels, the presence of additional sources in the field of view leads to inconsistent delay estimates from different channels. With sufficient signal to noise ratio, the star confusion can be then detected using chi-square statistics. An interesting result is that the star confusion can be detected even when the interferometer cannot resolve the separation between the target and confusion stars if their spectra are sufficiently different. Once detected, it is possible to mitigate the star confusion effect by incorporating the confusion effect in the data process.

In the following sections, we first present a general treatment of the star confusion effect. A simple first-order formula is derived for capturing leading the star confusion effect. We then describe the simulation configuration surveying over different star confusion scenarios and present the results of the impact on astrometric performance from single star confusion. Star confusion detection algorithm based on chi-squares statistics is presented. Finally, we show how to reduce the star confusion effect using a least-squares estimation of the star confusion effect and provide a summary at the end.

2. STAR CONFUSION MODELING

SIM's astrometric measurements are based on the fringe observations. When there are multiple stars in the field of view, the fringe signal has systematic errors due to the extra photoelectric signal generated by the confusion stars. Because the photons from different stars are incoherent, the fringe signal detected by a CCD pixel are simply the sum of the fringes generated by the stars in the field of view.

2.1. General formulation

SIM fringe measurements are obtained by dithering the delay line to modulate the fringe phase typically over about 1μm optical path difference (OPD) range. The total OPD equals the OPD from the phase modulation plus the external OPD* Suppose there are N_s confusion stars in the field of view. We label the target star as $s = 0$. Let $u(t)$ describe the modulation profile as function of time and d be the external OPD. The signal detected by a pixel at (m,n) in an M×N CCD for the i-th camera exposure is given by

$$y_i^{m,n} = \sum_{s=0}^{N_s} \int_{x_m}^{x_{m+1}} dx \int_{y_n}^{y_{n+1}} dy \int_{t_i}^{t_{i+1}} dt \int dk w\left(k, x, y, x_s(k), y_s(k)\right) I(k) \left\{1 + V(k)\cos[k(u(t)+d) + \phi(k)]\right\} \quad (1)$$

where x_m, y_n, $m = 1, 2, \cdots, M+1$ $n = 1, 2, \cdots, N+1$ represent the positions of the pixel boundaries along x and y directions; t_i's are the time sampling points. $I(k), V(k), \phi(k)$ are the intensity function†, visibility function, and the differential phase dispersion function respectively. $w(k, x, y, x_s, y_s)$ is a point spread function (PSF) describing the diffraction pattern of the instrument with (x_s, y_s) being the location of the geometric image of the s-th star on the CCD. The image of the center of the field of view for wave number k is located at $(x_0(k), y_0(k))$ on the CCD; the wave number dependency in functions $x_0(k)$ and $y_0(k)$ model the prism dispersing. For the same reason, the location of the geometric image of the confusion stars $(x_s(k), y_s(k))$ depends on k as well. Usually, the direction of the prism dispersing is aligned with one direction of the CCD pixel array, x or y. The pixel readings along the direction (column) perpendicular to the dispersing direction (row) are coadded. The spectral channels are formed by binning the consecutive columns of pixels. For a channel, the CCD reading is

$$Y_i = \int_{t_i}^{t_{i+1}} dt y^{\mathrm{ch}}(u(t) + d)\,. \quad (2)$$

Here $y^{\mathrm{ch}}(u)$ is the instantaneous fringe function detected by the channel

$$y^{\mathrm{ch}}(u) = \sum_{s=0}^{N_s} y_s(u), \quad y_s(u) = \sum_{m,n} \int_{x_m}^{x_{m+1}} dx \int_{y_n}^{y_{n+1}} dy \int dk w(k, x, y, x_s(k), y_s(k)) I(k) \left[1 + V(k)\cos(ku + \phi(k))\right] \quad (3)$$

where the sum is over the pixels (m,n) within the spectral channel; u is the OPD between the two arms of the interferometer. In fact, for stepping modulation Y_i is the same as $y^{\mathrm{tot}}(u_i)$ where u_i is the average value of $u(t)$ over the sampling interval $[t_i, t_{i+1}]$. For triangular modulation, Y_i is proportional to $y^{\mathrm{ch}}(u_i)$ up to a *sinc* factor

*To track the central fringe, the interferometer delay line is moved to compensate most of the external delay during operation.

†$I(k)$ should be understood as the product of the spectral energy function of the star, the instrument throughput, and the CCD detection efficiency.

that is very close to one for narrow bandwidth. We separate the fringe signals generated by the target star and the confusion stars by writing

$$y^{\text{tot}}(u) = y_0(u) + \sum_{s=1}^{N_s} y_s(u) \,. \tag{4}$$

The CCD readings Y_i's are then processed by the white light algorithms described in references.[5,6]

2.2. A simple model

It is heuristic to use a simple model to capture the main characteristics of the star confusion. The diffraction pattern $w(k, x, y, x_s, y_s)$ is a function centered at (x_s, y_s) with width being about the Airy spot size. The image spot $(x_s(k), y_s(k))$ moves along the dispersing direction monotonically as we vary k. The integration over k in (3) gets the main contribution from the region where $(x_s(k), y_s(k))$ is located in the geometric boundary of the spectral channel on the CCD extended by the size of the Airy spot. According to references,[5,6] for a narrow spectral channel, the broadband effect can be neglected[‡] by using a monochromatic fringe models

$$y_0(u) \approx I\,[1+V\cos(ku+\phi)]\,, \quad y_s(u) \approx I_s\,[1+V_s\cos(k_s(u+B\Delta\theta_s)+\phi_s)]\,, \tag{5}$$

where I, V, k, ϕ and I_s, V_s, k_s, ϕ_s are the effective intensities, visibilities, wave numbers, and dispersion phases for the target star and the s-th confusion star respectively. We note that k_s's and ϕ_s's are slightly different from k and ϕ for two reasons. First, the effective channel wave number and dispersion phase depends on the spectrum of the light source. Furthermore, the locations $(x_s(k), y_s(k))$ of geometric images of the confusion stars on the CCD are different because of their different locations in the field of view. B is the length of the baseline[§] and $\Delta\theta_s$ is the separation angle between the target and the s-th confusion star along the baseline. The effect of star confusion is not sensitive to the separation angle perpendicular to the baseline in the field of view. Because we are considering the star separation within a few arcseconds, the images of the confusion stars on the CCD are not shifted much from that of the target star. Also, the spectral dependency of the effective wave number and dispersion phase are weak for relatively narrow channel bandwidth. Therefore, it is a good approximation to assume

$$k_s \approx k\,, \quad \phi_s \approx \phi\,. \tag{6}$$

The superposition of monochromatic fringe signals can be conveniently viewed in terms of adding complex phasors, defined by

$$X \equiv IVe^{\imath\phi}\,, \quad X_s = I_s V_s e^{\imath\phi+\imath k\Delta\theta_s B}\,, \quad s = 1, 2, \cdots, N\,. \tag{7}$$

It is useful to define a relative confusion strength r_s

$$r_s \equiv I_s V_s/(IV) \tag{8}$$

to write the effect on the total phasor as an extra complex factor $\mathcal{V}^{\text{conf}}$

$$X^{\text{tot}} = \mathcal{V}^{\text{conf}} X\,, \quad \mathcal{V}^{\text{conf}} = \left(1 + \sum_{s=1}^{N_s} r_s e^{\imath k B\Delta\theta_s}\right)\,. \tag{9}$$

The phase of this extra factor is the phase error due to the star confusion. The visibility is altered by multiplying the magnitude of $\mathcal{V}^{\text{conf}}$. Therefore, when there are multiple stars in the field of view, the total effect on the astrometric performance may be viewed as a superposition of the effect due to each individual star expressed as "phasors". This is consistent with reference.[9] For weak confusions, $r_s \ll 1$,

$$\text{Arg}\{\mathcal{V}^{\text{conf}}\} \approx \sum_{i=s}^{N_s} r_s \sin(k\Delta\theta_s B)\,. \tag{10}$$

[‡]In fact, only for narrow angle science, where the accuracy in OPD estimation is at picometer level, the broadband effect is significant. For dim science, which the star confusion study is mostly for, using eight or more spectral channels over 400nm-1000nm, the error due to ignoring the broadband effect is in tens of picometers, thus negligible for dim science error budget.

[§]More precisely, B should be the length of the projection of the baseline perpendicular to the observation direction.

Expression (10) shows that the fringe phase error due to multiple stars is simply a linear superposition of the the phase errors due to the individual stars for weak confusion cases. The weak confusion assumption holds usually for the confusion cases we are mostly concerned because otherwise the confusion star has to be very bright and close to the target, which we try to avoid.

We now examine closely the case of a single star confusion, *i.e.* $N_s = 1$. The phase error due to a single star confusion is expressed as

$$\delta\phi = \mathrm{Arg}\{\mathcal{V}^{\mathrm{conf}}\} = \tan^{-1}\frac{r\sin(k\Delta\theta B)}{1+r\cos(k\Delta\theta B)}\,, \tag{11}$$

where we have dropped the subscripts labeling the confusion star $r = r_1$. When the separation of the confusion and target stars are small that their central fringes overlap, ratio r equals simply the relative spectral energy intensity of the confusion star with respect to the target star. As the separation becomes larger, the confusion star's fringe visibility is suppressed by the fringe envelope assuming tracking the central fringe of the target star. Therefore,

$$r = \left(I^{\mathrm{conf}}/I\right) f^{\mathrm{env}}(\Delta\theta B)\,, \tag{12}$$

where $f^{\mathrm{env}}(\Delta\theta B)$ is the coherence envelope function of the confusion star fringe and I^{conf} and I are the channel intensities of the confusion and the target stars respectively. By definition, the ratio I^{conf}/I scales exponentially with the visual magnitude difference between the confusion and target stars,

$$r = r_{\mathrm{spec}}10^{-0.4\Delta m}\,. \tag{13}$$

For weak single star confusion, $r \ll 1$, we get a simple formula for the star confusion effect on the fringe phase estimation

$$\delta\phi \approx r\sin(kB\Delta\theta) \tag{14}$$

$$\approx r_{\mathrm{spec}}10^{-0\ 4\Delta m} f^{\mathrm{env}}(\Delta\theta B)\sin(k\Delta\theta B)\,. \tag{15}$$

Phase estimation error due to star confusion depends on the separation angle via two factors, the fringe coherence envelope factor that suppresses the star confusion at the large separation angles and a sine factor that changes rapidly as function of the separation angle. This sine factor also shows that when the confusion star is very close to the target star, the star confusion effect is approximately linear in the separation angle.

2.3. Channel delays

Suppose the CCD is partitioned into N spectral channels. Expression (14) for weak single star confusion holds for the phase estimation from each spectral channel. To the leading order, the channel delay estimates for single star confusion may be modeled as

$$d_n = d_0 + \frac{r_n}{k_n}\sin(k_n B\Delta\theta) \quad n = 1, 2, \cdots, N \tag{16}$$

where d_0 is the true OPD; $\Delta\theta$ is the angular separation between the confusion and target stars; k_n and r_n are the channel wave number and the relative signal ratio between the confusion fringe and the target fringe for the nth channel. In view of (12), r_n's are proportional to the confusion star intensity and also depend on the separation angle via the coherence envelope function. Here the subscript n labels the spectral channels.

2.4. Simulation configuration

To be more rigorous, we use a simulation tool, the Star LIght Model (SLIM)[7] to study the impact on the astrometric performance due to star confusion. The CCD is modeled as a two dimensional array of pixels detecting the integration of the photon flux over each pixel's area and the duration of the camera exposure. The point spread function (PSF) describing the diffraction pattern is the Fourier transform of the SIM annular pupil, which takes the the form[8]

$$w(k,\rho) = \frac{1}{\pi(1-\gamma^2)}\left[\frac{J_1(ka\rho) - \gamma J_1(k\gamma a\rho)}{ka\rho}\right]^2\,, \tag{17}$$

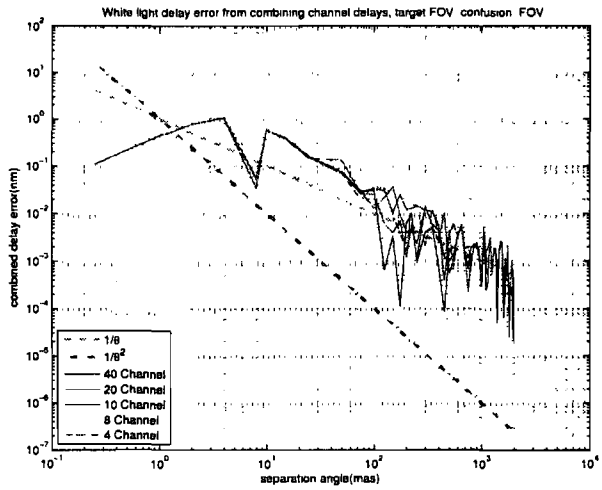

Figure 1. White light OPD error using different number of spectral channels.

where ρ is the angular distance from the center of the diffraction pattern or the geometric image point; k is the wave number; a and γa are the radius of the outer and inner radii of the annular aperture. Diffraction pattern (17) satisfies normalization condition

$$\int dx \int dy\, w(k, \sqrt{x^2+y^2}/(ka)) = 1\,. \tag{18}$$

SIM aperture size is $a = 30.45cm$. We assume that the inner radius is half of the outer radius, *i.e.* $\gamma = 0.5$. For SIM optics, a single CCD pixel is a square with the length of each side corresponding to $10\mu rad$ in the sky. We simulated four 80×5 CCDs with the prism dispersing along x direction having extension of 80 pixels. With the two polarization beam splitters at the two combiner sides, SIM instrument generates four sets of fringes detected by the four CCDs separately. The extension of y dimension is 5 pixels. A linear dispersing function is used to map the wave numbers for bandwidth 400nm–1000nm uniformly to the 80 pixel range on the CCD.

The results on the astrometric performance to be presented in the next section are generated without including a field stop. A field stop simply suppresses the star confusion from large separation angles that are out of the opening of the field stop. We use the star spectra template from the Pickles spectra database[10] for both the target and confusion stars. Our simulation uses perfect angle tracking because the OPD error due to star confusion is not sensitive to small angle tracking errors less than 100mas, which is true in most of the cases as reported in reference.[4] For 100 mas angle tracking error, only a few picometers in the white light OPD after combining the channel OPDs.

3. SIMULATION RESULTS OF THE IMPACT OF STAR CONFUSION

In this section, we present the results from the simulation of a single star confusion. We note that the impact to the astrometric performance is not sensitive to how many spectral channels are used. This may be seen from Figure 1, which displays the white light OPD errors as functions of the separation angle using 4, 8, 10, 20, and 40 spectral channels over bandwidth 400nm-1000nm. At large separation angle, it is suppressed by the coherence envelope function. The highly oscillational behavior and the linear behavior for small separation angle come from the factor $\sin(k\Delta\theta_s B)$. The white light OPD is formed by combining the channel OPDs from all the channels. Using wider channels can be viewed as combining more fringe signals before applying the OPD estimation algorithms while using narrower channels means more combination is done to the channel OPDs. Because the system is approximately linear, combining fringe signals does not differ much from combining the delays. Therefore, the white light OPD errors are not sensitive to the number of spectral channels used. Our

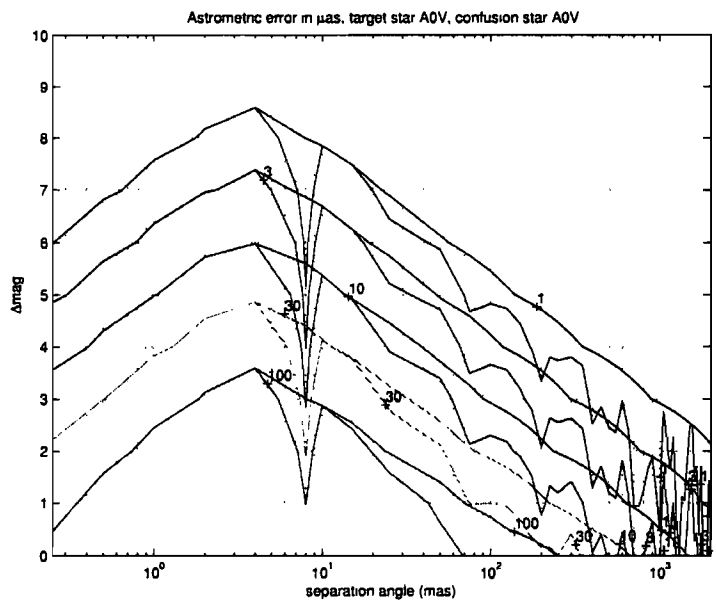

Figure 2. Astrometric error due to a single A0V star confusion for an A0V target star

results for the impact on the astrometric performance are computed as the RMS of the errors using 4, 8, 10, 20, and 40 channels.

The main factors relevant to the star confusion effect are the separation angle along the baseline and the visual magnitude and spectral difference between the target and confusion stars. Our simulation surveys over four arbitrarily picked spectral types, namely A0V, F0V, M0V, and K5III star types for both the target and confusion stars. For each target and confusion spectral type pair, the result is presented as contour plots in the magnitude difference Δm and the separation angle $\Delta\theta$ plane. Each contour represents the line with constant astrometric error in unit of μas. The original contours were very rough due to the rapidly oscillating sine factor dependency on the separation angle. Since we are more interested in the upper bound of the error, we have drew the new smooth contours as an upper bound of the rough contours. Figure 2 shows the process. The smooth contours overestimate the impact of the confusion star on the astrometric performance.

Figures 3 shows the contours of the astrometric errors due to an A0V star confusion for a target star of types A0V, F0V, K5III, and M0V respectively.

An empirical fitting formula in form

$$\text{Astrometric error} = 10^{-0.4\Delta m}\frac{a\Delta\theta}{1 + b\Delta\theta + c\Delta\theta^2} \tag{19}$$

is valid for the weak confusion case. In Table 1, we display the coefficients a, b, c for the cases under study. It appears that a confusion star of type K5III causes more impact than an A0V star of the same magnitude. This is due to the fact that, for the same visual magnitude, a K5III star has more photons than an A0V star because the visual magnitude is defined using the spectral energy over a spectral window around 450nm.

4. CONFUSION DETECTION USING χ^2-STATISTICS

In order to detect the star confusion, we need to use the delay estimations from multiple channels. In view of model (16), the existence of star confusion causes the delay estimates from different channels to be inconsistent. See Figure 4. Given sufficient SNR, the discrepancy of the channel delay estimates can be used to detect the star confusion. We do hypothesis testing based on the χ^2-statistics. The null hypothesis is that no confusion star is

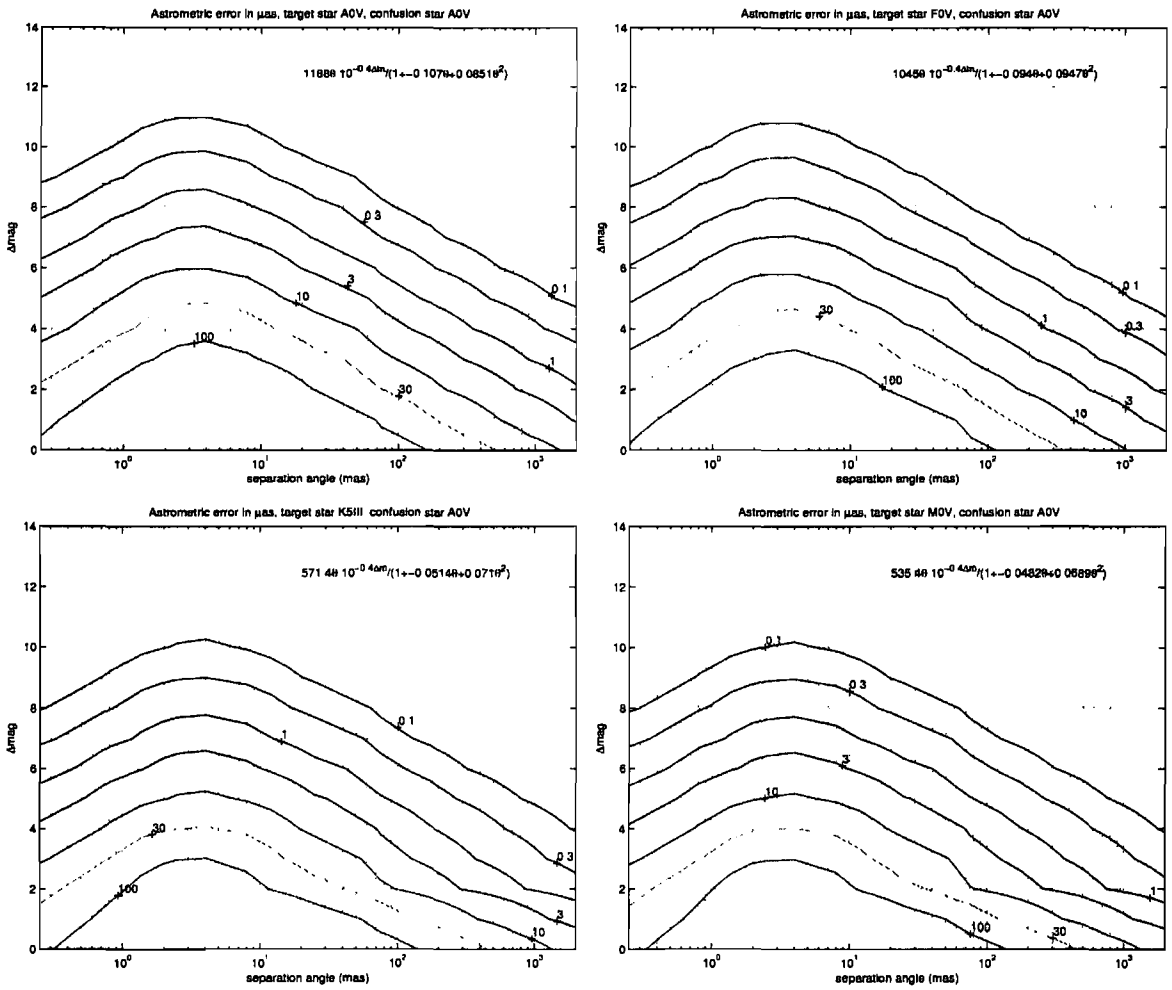

Figure 3. Astrometric error due to single A0V star confusion for different target stars

Table 1. Coefficients a, b, and c, from fitting to formula (??).

Confusion star types	Target star types			
	A0V	F0V	K5III	M0V
A0V	a = 1188 b = -0.107 c = 0.0851	a = 1210 b = -0.109 c = 0.0609	a = 2601 b = -0.234 c =0.0426	a = 2906 b = -0.262 c = 0.0408
F0V	a = 1045 b = -0.094 c = 0.0947	a = 1317 b = -0.119 c = 0.101	a = 2024 b = -0.182 c =0.0459	a = 2259 b = -0.203 c = 0.044
K5III	a = 571 b = -0.0514 c = 0.0851	a = 620 b = -0.0558 c = 0.0689	a = 1276 b = -0.115 c =0.0955	a = 1201 b = -0.108 c = 0.0739
M0V	a = 535 b = -0.0482 c = 0.0689	a = 578 b = -0.052 c = 0.067	a = 1238 b = -0.111 c =0.104	a = 1272 b = -0.114 c = 0.0949

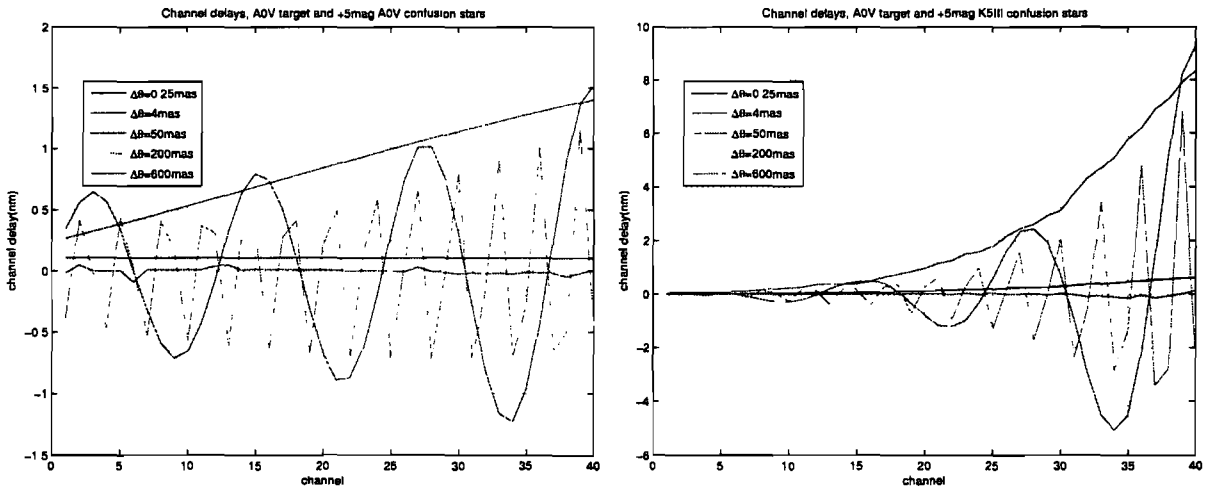

Figure 4. Channel delays for an A0V target star with a 5 magnitude dimmer A0V and K5III confusion star

in the field of view. The delay estimates from all the channels are the same to the noise level because r_n's are all zero. With the existence of photon shot noise and measurement read noise, the delay all fluctuates about d_0 with certain standard deviation σ_n's. We first fit d_n's to a constant value d_0 by minimizing

$$\chi^2 = \sum_{n=1}^{N} \frac{(d_n - d_0)^2}{\sigma_n^2} . \tag{20}$$

Varying Eq. (20) with respect to d_0 gives the value of d_0 that minimizes (20),

$$d_0^{\min} = \sum_{n=1}^{N} \frac{\sigma^2}{\sigma_n^2} d_n , \quad \sigma^2 = \left(\sum_{n=1}^{N} \frac{1}{\sigma_n^2} \right)^{-1} . \tag{21}$$

Note that σ is the standard deviation of $d_0^{\min}$. The minimal value of χ^2 (the residual)

$$\chi^2_{\min} = \sum_{n=1}^{N} \frac{(d_n - d_0^{\min})^2}{\sigma_n^2} \tag{22}$$

satisfies approximately a χ^2-distribution[¶] with $N-1$ degrees of freedom.[11] The alternative hypothesis is that the channel delays are biased due to star confusion. The residual $\chi^2_{\min}$ satisfies a noncentral χ^2-statistics with the bias λ

$$\lambda \equiv \min_{\epsilon_0} \sum_{n=1}^{N} \frac{(\epsilon_n - \epsilon_0)^2}{\sigma_n^2} = \sum_{n=1}^{N} \frac{(\epsilon_n - \epsilon_0^{\min})^2}{\sigma_n^2} , \quad \epsilon_0^{\min} = \sum_{n=1}^{N} \frac{\sigma^2}{\sigma_n^2} \epsilon_n , \tag{23}$$

where ϵ_n's are the systematic channel delay errors due to the star confusion. See appendix A for details of the noncentral χ^2-statistics. When the bias λ is large enough, the two distributions are separated so that it is possible to define a detection algorithm to have small type I and II errors corresponding to the false and missed detection errors. Note that bias λ increases as we decreases the channel delay variances σ_n^2. Therefore, with sufficient SNR, the detection of the star confusion is possible. Figure 5 shows the probability density functions of the χ^2- and noncentral χ^2-distributions for 39 degrees of freedom, which is relevant for using 40 spectral channels. If we use the dashed vertical line as the boundary of the critical region (the area with cyan color) for the hypothesis testing, the probability of having type I error (false rejection of the null hypothesis) is $\alpha = 5\%$. The probability of having type II error (false acceptance of the null hypothesis) is $\beta = 5\%$.

[¶]This is exact when d_n's satisfy normal distributions.

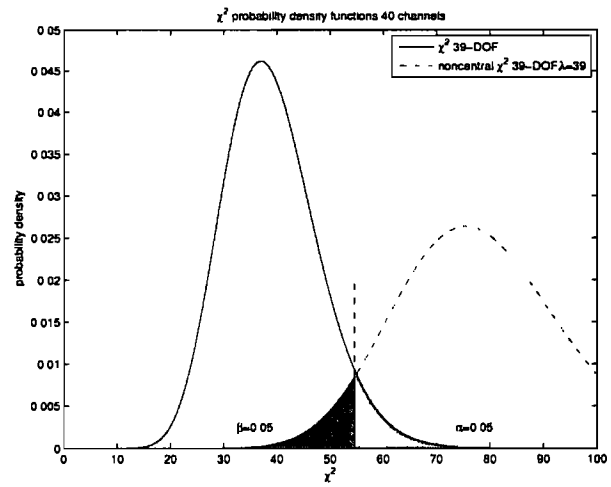

Figure 5. Probability distribution functions for χ^2- and noncentral χ^2-statistics

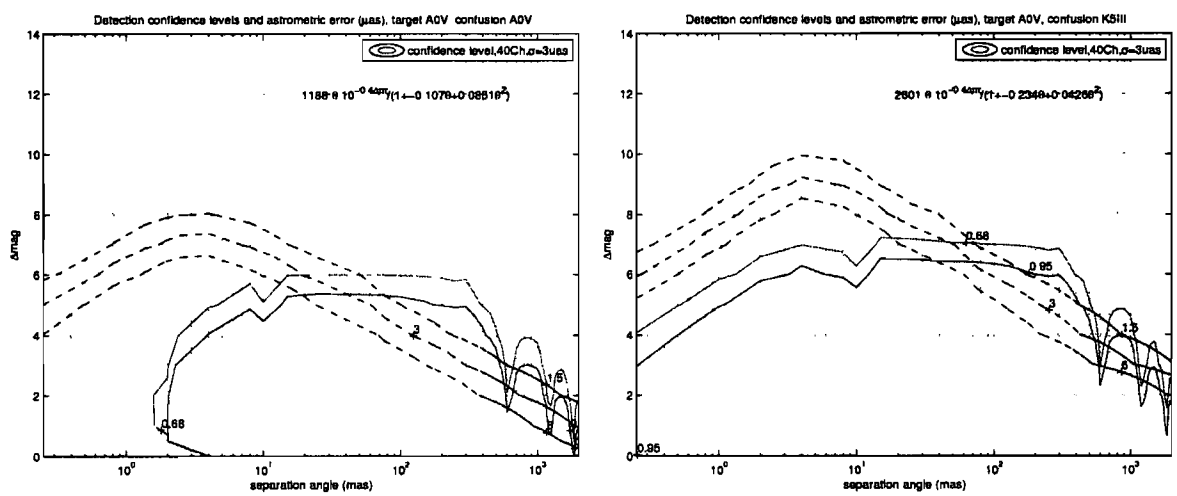

Figure 6. Contours of confidence levels for detecting an A0V and K5III confusion around an A0V target star

Unlike the white light OPD errors due to star confusions, the confusion detection depends on the number of channels. In Figures 6, we display the confidence level contours at 95% and 68% for star confusion detection (with both type I and II errors less than 5% and 32% respectively) on the star magnitude difference and separation angle plane using 40 spectral channels. Putting the read noise aside, it is always preferred having as many channels as possible. Besides, with more spectral channels, the channel signals can always be combined to mimic the case of using less spectral channels. However, the read noise, whose variance is about 25 for SIM, are unavoidable. Therefore, the number of channels to use should be determined by a balance between using more channels to gain more information and having less readings to reduce the read noise. From now on, our analysis assumes using 40 spectral channels. An interesting result is that even though a binary star system is not resolved by the interferometer in the sense that

$$B\Delta\theta k \ll 1 \tag{24}$$

it is still possible to detect the binary system if the two stars have different spectra as shown in Figure 6. When the two stars have different spectra, the optical centers for the spectral channels are different. Therefore, it is

possible to detect a binary star system with an interferometer with multiple spectral channels even when the binary system is unresolved.

5. MITIGATE SINGLE STAR CONFUSION EFFECT

Once detected, it is possible to mitigate the star confusion effect. Assuming a single star confusion scenario, we can fit the channel delays to the model (16). However, because the relative intensities of the channel signals, r_i's, are typically unknown, a parameterization is needed to reduce the degrees of freedom. We shall assume that r_i's as function of the channels is approximately an mth order polynomial,

$$r_n = \sum_{p=0}^{m} a_p k_n^p \,. \tag{25}$$

Practically, we should consider only lower order polynomials. When $\Delta\theta$ is small, we can not achieve much because the channel dependency due to factor $\sin(k_n B\Delta\theta)$ can be hardly distinguished from r_n. When the separation angle is so small that the interferometer can not resolve it, we have $k_n B\Delta\theta \ll 1$ and

$$d_n \sim d_0 + r_n B\Delta\theta \,. \tag{26}$$

A binary system consisting two stars having similar spectra with the separation unresolved by the interferometer looks like just a single star to the interferometer. If the two stars have different spectra, r_n's are different for different channels. It is possible to detect the confusion even though the separation between the confusion star and target star are not resolved by the interferometer as discussed in the previous section. However, without any spectral knowledge, it is hard to find out the angular separation between the two stars and d_0. With the spectral knowledge, a linear fit using (26) yields the star separation angle $\Delta\theta$ and d_0.

We emphasize that $\Delta\theta$ is the separation angle along the baseline of the interferometer. In case the two stars are separated along the direction perpendicular to the baseline, a different orientation of the baseline would make $\Delta\theta$ large enough so as to be resolved by the interferometer. We now assume that the confusion star is resolved by the baseline so that the factor $\sin(k_n B\Delta\theta)$ oscillates several cycles across the channels. In this case, the oscillation period may be used to find out the separation angle $\Delta\theta$. The crudest approximation is treating all the r_n's as the same, *i.e.* $m = 0$. Practically, we consider the order up to 2 in approximation (25). We write the delay model as

$$\phi = M(\Delta\theta)x \tag{27}$$

where vector ϕ contains the delay phases from N spectral channels,

$$\phi = [k_1 d_1, k_2 d_2, \cdots, k_N d_N]^T \,, \tag{28}$$

vector x consists the unknown variables d_0 and the polynomial coefficients a_p's,

$$x = [d_0, a_0, a_1, \cdots, a_m]^T \,, \tag{29}$$

and matrix $M(\Delta\theta)$ is given by

$$M(\Delta\theta) = \begin{pmatrix} k_1 & \sin(k_1\Delta\theta B) & k_1\sin(k_1\Delta\theta B) & \cdots & k_1^m\sin(k_1\Delta\theta B) \\ k_2 & \sin(k_2\Delta\theta B) & k_2\sin(k_2\Delta\theta B) & \cdots & k_2^m\sin(k_2\Delta\theta B) \\ \vdots & \vdots & \vdots & \vdots & \vdots \\ k_N & \sin(k_N\Delta\theta B) & k_N\sin(k_N\Delta\theta B) & \cdots & k_N^m\sin(k_N\Delta\theta B) \end{pmatrix} . \tag{30}$$

We can find the separation angle $\Delta\theta$, d_0, and a_p, $p = 0, \cdots, m$ by fitting the model (27) to the estimated channel phases. A least-squares fitting is formulated as

$$\min_{\Delta\theta, x} |\phi - M(\Delta\theta)x|^2 \,. \tag{31}$$

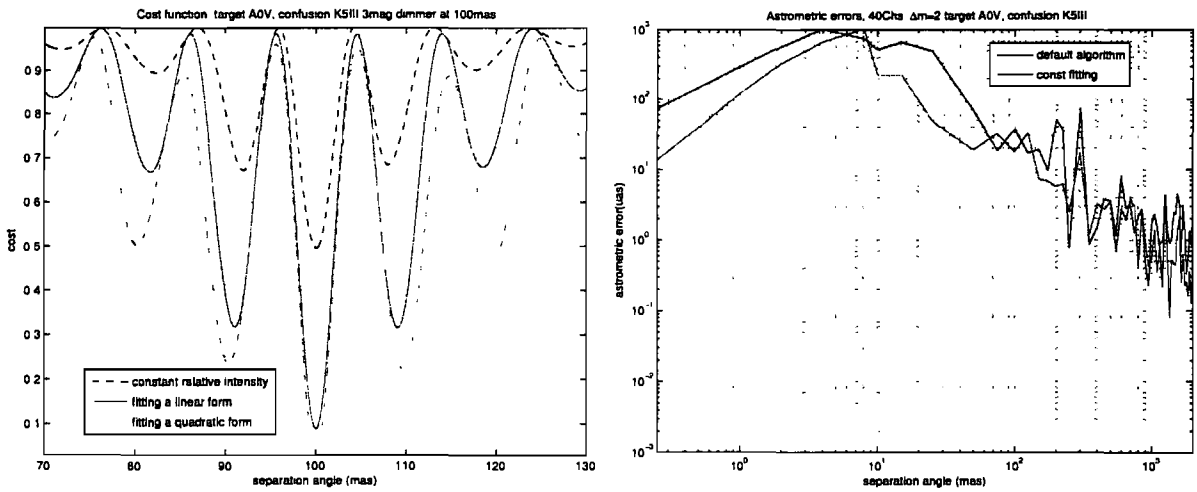

Figure 7. Cost functions without noise for A0V target star with star confusion from a K5III star (left) and astrometric error with and without incorporating the star confusion in the data processing.

It can be reduced to a one-dimensional nonlinear fitting by solving

$$x(\Delta\theta) = M(\Delta\theta)^{\dagger}\phi \tag{32}$$

for a given $\Delta\theta$. Substituting x in the minimization cost function using (32) gives

$$\min_{\Delta\theta} \left|\phi - M(\Delta\theta)M(\Delta\theta)^{\dagger}\phi\right|^2 . \tag{33}$$

Matrix $M(\Delta\theta)M(\Delta\theta)^{\dagger}$ is a projection operator to the range space of $M(\Delta\theta)$, which may be evaluated by using a QR-decomposition $QR = M(\Delta\theta)$. The minimization problem (33) is equivalent to maximizing the norm of $Q\phi$. The optimal value $\Delta\theta_m$ gives an estimation of the location of the confusion star. In Figure 7, we display the cost function (33) as functions of the separation angle $\Delta\theta$ for star confusion cases where the target and confusion stars have same and different spectral types without including any noise in the left plot. The three curves correspond to the polynomial approximation (25) at orders $m = 0, 1, 2$ respectively. For each curve, we can identify clearly the minimum of the cost function. When the confusion star (of type K5III) and the target star (of type A0V) are of different spectral types, the optimal value of the cost function for $m = 0$ is only 0.5 because it is not a good approximation to assume that r_n's are all the same. However, the location of the minimum is at the correct separation angle. We can see that using $m = 0$ or a constant fitting gives adequate performance in finding the separation angle between the two stars. With this, we can define an optimization problem to minimize the impact from the confusion star at $\Delta\theta$. For example, using relation (32) gives the estimated d_0. The second plot in Figure 7 shows the delay errors after applying the confusion fitting algorithm using a linear approximations for r_n's. We can see consistent improvement in the separation angle range between 10mas to 100mas. However, fitting more parameters may increase the sensitivity to noises. Therefore, a thorough analysis should include the noise sensitivity.

6. SUMMARY AND CONCLUDING REMARKS

We have studied the impact of star confusion on the SIM astrometric performance focusing on the fringe data process. The impact due to a single star confusion for spectral types A0V, F0V, K5III, and M0V with different visual magnitude differences are quantified. Star confusion from multiple stars may be analyzed as a linear superposition of a conveniently defined phasors. The impact of the star confusion is proportional to the intensity of the confusion star and a relatively complicated function of the separation angle including a highly oscillational behavior and the fringe envelope suppression effect. The impact due to star confusion is neither sensitive to small

angle tracking errors nor to the number of spectral channels used. It is possible to detect the star confusion using χ^2-statistics with fringe measurements from multiple spectral channels. Within the error budget for the read noise, we should use as many spectral channels as possible for star confusion detection because we gain more information by using more channels; it is always possible to form fringe signals of wider channels by combining fringe signals from narrower channels. Finally, we described a simple least-squares fitting algorithm based on single star confusion model for finding the location of the confusion star and reducing the astrometric error due to confusion.

In the future, we can extend this study to the cases for more realistic observation scenarios. We need look for more sophisticated data analysis methods suitable for mitigating the impact from the star confusion. Noise sensitivity analysis should be included. In this memorandum, we only considered the fringe measurements for a single baseline orientation. When combining the observations from multiple baselines, we expect analysis of the synthesized data can effectively reduce the astrometric error due to confusion. With multiple baselines, it is also possible to detect multiple star confusions and estimate the locations of the confusion stars by fitting to a multiple star confusion model.[12,13]

Acknowledgments

We would like to thank Hong Tang and Tsae-pying Shen for reviewing our manuscript. This work was prepared at the Jet Propulsion Laboratory, California Institute of Technology, under a contract with the National Aeronautics and Space Administration.

APPENDIX A. χ^2-AND NONCENTRAL χ^2-DISTRIBUTIONS

For the purpose of reference, we include here the probability functions of the χ^2-distribution for N degrees of freedom

$$p_N(\chi^2) = \frac{(\chi^2)^{N/2-1} \exp\left(-\chi^2/2\right)}{\Gamma(n/2)2^{n/2}} \tag{34}$$

and the non-central χ^2-distribution[14] for N degrees of freedom

$$p_N(\chi^2, \lambda) = \frac{(\chi^2)^{N/2-1} \exp\left(-(\chi^2+\lambda)/2\right)}{2(\sqrt{\lambda\chi^2})^{N/2-1}} I_{n/2-1}(\sqrt{\lambda\chi^2}), \tag{35}$$

where the bias λ is given by

$$\lambda \equiv \sum_{i=1}^{N} \frac{b_i^2}{\sigma_i^2} \tag{36}$$

with b_i and σ_i are the bias and standard deviation of the ith degree of freedom respectively.

REFERENCES

1. J. Marr, "Space Interferometry Mission(SIM) overview and current status," *SPIE conference on Interferometry in Space* **4852**, pp. 1–15, 2002.
2. R. A. Laskin, "SIM technology development overview-light at the end of the tunnel," *SPIE conference on Interferometry in Space* **4852**, pp. 16–32, 2002.
3. C. W. Allen, *Astrophysical Quantities*, The Athlone Press, London, Reprinted, 1991.
4. N. Fathpour, *Centroiding Estimates of the Angle tracking camera in presence of a confusion field for SIM–Space Interferometry Mission*, SPIE conference 2007.
5. M. Milman, C. Zhai, and M. Regehr, "White light interferometry using a channel spectrum part 1: model,algorithm," *submitted to Applied Optics*, 2006.
6. C. Zhai, M. Milman, M. Regehr, and P. Best, "White light interferometry using a channel spectrum part 2: calibration methods, numerical and experimental results," *submitted to Applied Optics*, 2006.

7. M. Regehr and M. Milman, "Analysis and numerical modeling of error sources in SIM star light phase detection," *IEEE Aerospace Conference, Big Sky, MT*, No. 1356, 2005.
8. M. Born and E. Wolf, *Principle of Optics*, Sixth Edition, Pergamon Press, Oxford, 1989.
9. J. Rajagopal, T. Böker, and R. Allen, *The confusion limit on astrometry with the Space Interferometry Mission*, Publications of the Astronomical Society of the Pacific, **113**, pp1232-1242, October, 2001.
10. A. J. Pickles, "A stellar spectral flux library: 1150 - 25000Å," *Publ. Astron. Soc. Pac.* **110**, pp. 863–878, 1998.
11. S. L. Meyer, *Data analysis for scientists and engineers*, John Wiley&Sons, Inc, New York, 1975.
12. J. Yu, S. Shaklan, and M. Shao, *High precision Astrometry of Crowded Fields by Interferometry*, SPIE, **1947**, pp. 209-217, 1993.
13. N. Dalal and K. Griest, *Astrometric imaging of crowded fields with only two SIM pointings*, AstroPhysics, January, 2001.
14. N. L. Johnson and S. Kotz, *Continuous Univariate Distributions*, vol. 2, Houghton-Mifflin, 1970.
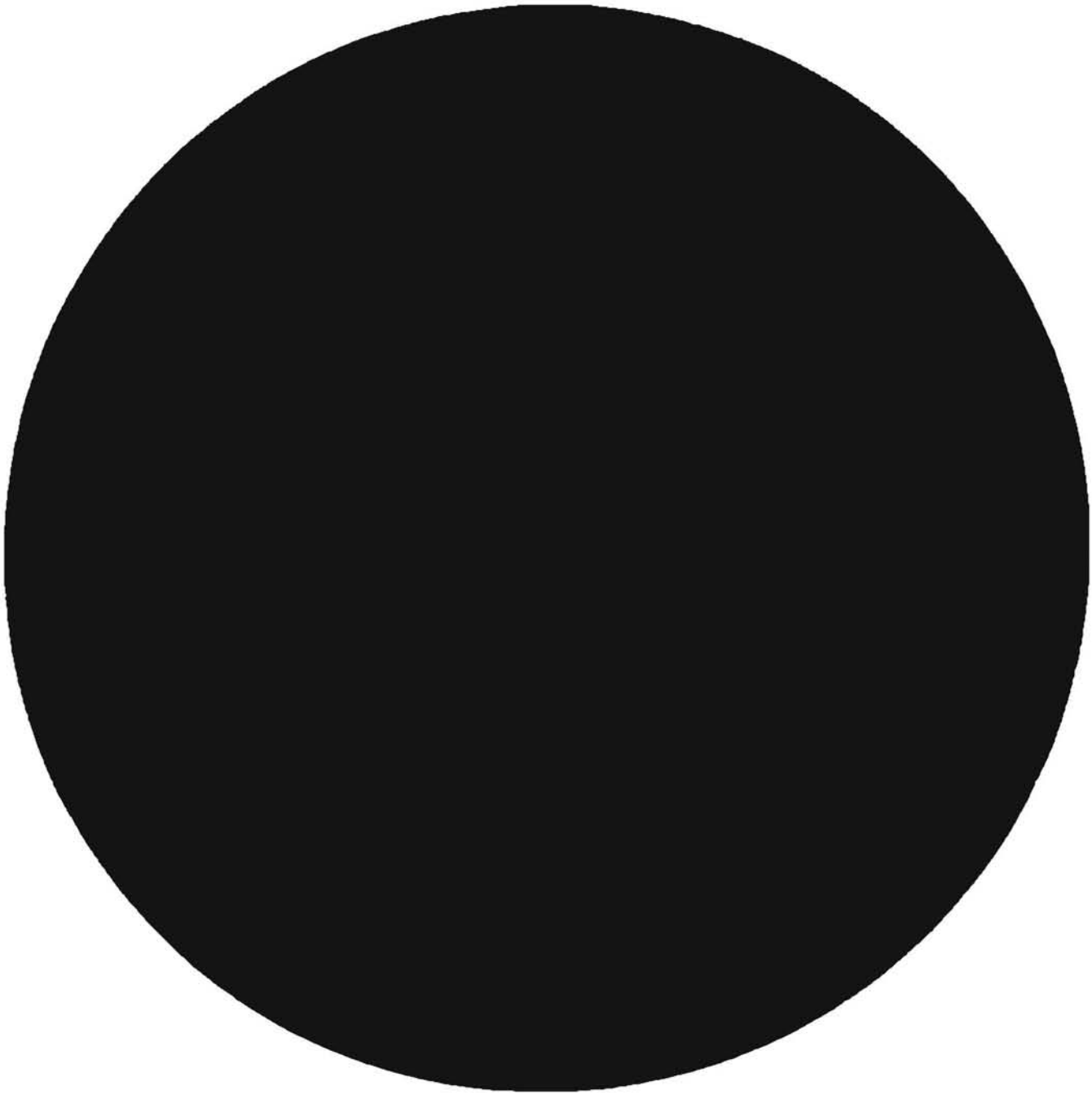
End of File